


Research Article

Open Access



Construction and ultrasonic inspection of the high-capacity Li-ion battery based on the MnO₂ decorated by Au nanoparticles anode

Cuihua An¹, Shikang Wang¹, Liyang Lin³, Xiangyan Ding¹, Qibo Deng¹ , Ning Hu^{1,2}

¹School of Mechanical Engineering, and School of Materials Science and Engineering, Hebei University of Technology, Tianjin 300401, China.

²State Key Laboratory of Reliability and Intelligence Electrical Equipment, Key Laboratory of Advanced Intelligent Protective Equipment Technology, Ministry of Education, Hebei University of Technology, Tianjin 300130, China.

³Chongqing Key Laboratory of Green Aviation Energy and Power, Chongqing 401130, China.

Correspondence to: Prof. Qibo Deng, School of Mechanical Engineering, Hebei University of Technology, Tianjin 300401, China. E-mail: qibodeng@hebut.edu.cn

How to cite this article: An C, Wang S, Lin L, Ding X, Deng Q, Hu N. Construction and ultrasonic inspection of the high-capacity Li-ion battery based on the MnO₂ decorated by Au nanoparticles anode. *Microstructures* 2024;4:2024003. <https://dx.doi.org/10.20517/microstructures.2023.64>

Received: 27 Oct 2023 **First Decision:** 28 Nov 2023 **Revised:** 11 Dec 2023 **Accepted:** 28 Dec 2023 **Published:** 8 Jan 2024

Academic Editor: Yida Deng **Copy Editor:** Fangling Lan **Production Editor:** Fangling Lan

Abstract

Lithium (Li)-ion batteries have become one of the main energy sources for electric vehicles and energy storage systems, which puts forward higher requirements for the detection of battery state of health (SOH). The SOH of batteries is crucial for areas such as battery management and renewable energy storage. Accurately evaluating the SOH of batteries can optimize charging and discharging strategies and extend battery life. Therefore, accurately and effectively monitoring the SOH of Li batteries is of great significance. An ultrasonic testing technology has been proposed that can non-destructively test the Li battery SOH, enabling accurate judgment of batteries in poor or damaged conditions. Firstly, the hetero-structured MnO₂-Au has been constructed as the anode for Li-ion batteries. MnO₂-Au heterojunction enhances electronic conductivity and ion conductivity. The MnO₂-Au has exhibited high specific capacity and superior rate performances, which can well satisfy the ultrasonic inspection of the battery. Then, the ultrasonic testing has been conducted on batteries with different ages. The results suggest that batteries with short circuits have the highest nonlinear coefficient, while batteries with short circuits after long cycles have the lowest nonlinear coefficient. The nonlinear coefficient of batteries with different charging and discharging states is in the middle.

Keywords: Lithium-ion batteries, non-destructive testing, ultrasound technology, health status



© The Author(s) 2024. **Open Access** This article is licensed under a Creative Commons Attribution 4.0 International License (<https://creativecommons.org/licenses/by/4.0/>), which permits unrestricted use, sharing, adaptation, distribution and reproduction in any medium or format, for any purpose, even commercially, as long as you give appropriate credit to the original author(s) and the source, provide a link to the Creative Commons license, and indicate if changes were made.



INTRODUCTION

As an important energy storage device, lithium (Li) batteries are widely used in electric vehicles, mobile devices, energy storage systems, and other fields^[1-4]. However, these batteries encounter many problems during operation, including capacity decay, internal resistance increase, temperature rise, and so on. These issues may lead to a decrease in their performance and lifespan, as well as potential risks of spontaneous combustion and explosion and even serious damage to human life and property^[5,6]. Therefore, the accurate detection of the state of health (SOH) of Li batteries is extremely important in practical applications. The SOH of Li batteries can test some key parameters such as capacity, internal resistance, and temperature, so as to detect the problems within the batteries and provide timely maintenance suggestions for users^[7-9]. If the degree of attenuation in the Li batteries can be accurately known during the recycling process, the recycling procedure of these batteries can be realized step-by-step, which would reduce the waste of the social resources^[10,11].

The traditional health detection method for Li batteries is to calculate and evaluate their SOH through the battery management system (BMS)^[12,13]. The key factors of these batteries, including temperature, current, and voltage, are usually monitored, which have been used to control their charging/discharging process to protect the safety and stability of the Li batteries. However, it is difficult for the BMS estimation system to detect the Li batteries in the early stage, especially the subtle changes inside them, which makes the detection conservative and makes it difficult to judge sudden failures^[14,15]. In addition, microscopy techniques are also widely used in the characterization of the internal microstructure of the Li batteries, including scanning electron microscopy (SEM), optical microscopy, transmission electron microscopy, and so on, which can analyze the different health states of the Li batteries^[16-19]. However, the above method requires the disassembly of these batteries, which may cause damage to the interfacial structure between the solid electrolyte and the electrode. Additionally, the electrode materials are easily contaminated during the transfer procedure, leading to inaccurate results. In recent years, various technologies, such as sensors, magnetic resonance, X-ray scanning imaging, ultrasonic testing, and Raman scattering, have been widely used in the non-destructive testing and monitoring of the Li batteries by virtue of their ability to deeply study the real-time data on battery operating status^[20-23]. As one of the non-destructive testing methods, ultrasonic testing has the advantage that it can detect changes inside the Li battery accurately in real time without causing any damage, especially the small changes, including the gas production, electrolyte wetting, Li distribution, overcharge, short circuit, and so on^[14,24,25]. In addition to identifying the structural problems, the ultrasound wave can also determine whether the SOH of the Li batteries is reliable, thereby reducing maintenance costs and improving battery life. Therefore, ultrasonic technology will become an important tool in the field of battery online monitoring and fault diagnosis. The application of ultrasonic testing in battery health testing falls into two major categories. One is to use the transmission of sound waves inside Li batteries to obtain the physical information of the electrode material. The other is based on acoustic emission technology to detect the internal state of these batteries. The electrode material is used as the source of acoustic emission, which is detected by an ultrasonic probe attached to the sample. After analysis by the signal processing system, batteries with different health states are obtained^[26].

This work mainly utilizes ultrasonic testing technology to analyze Li batteries in different states. By analyzing ultrasound signals and obtaining normalized ultrasound nonlinear coefficients, the battery SOH can be determined. Firstly, heterogeneous MnO₂-Au materials have been constructed as the Li battery anode for ultrasonic testing. The MnO₂-Au anode exhibits high specific capacity and superior rate performances, satisfying the ultrasonic experiments of the Li battery. Then, the ultrasonic testing has been conducted on these batteries with different ages. Moreover, the batteries with short circuits have the highest nonlinear coefficient, while those with short circuits after long cycles have the lowest nonlinear coefficient. The nonlinear coefficient of the batteries with different charging and discharging states is in the middle.

EXPERIMENTAL

Preparation

MnO₂ samples

A certain amount of KMnO_4 and MnSO_4 were dissolved in deionized water under thorough stirring, respectively. Subsequently, the above two solutions were mixed and stirred vigorously for 10 min. The resulting solution was then poured into an autoclave, which was maintained at 200 °C for 5 h. After cooling to 25 °C, the initial sample was collected and washed several times. The black sediment was collected after centrifugation. Finally, after drying and grinding, the MnO_2 samples were collected.

Preparation of MnO_2 -Au samples

First, a specified volume of MnO_2 samples was tipped into deionized water, which was stirred to form a black suspension. Secondly, 1.425 mL HAuCl_4 aqueous solution was dropped into the above solution under stirring. Subsequently, a specified volume of NaBH_4 aqueous solution was slowly tipped to the mixed solution under stirring. The resulting gray-black product was collected and washed several times. Finally, The MnO_2 -Au samples were dried under vacuum.

Characterization

The constitution, micro-morphologies, and valences of the obtained MnO_2 and MnO_2 -Au were analyzed using X-ray diffraction (XRD, Rigaku Ultima IV), SEM (Verios 460I, FEI), and X-ray photoelectron spectroscopy (XPS, ESCACAB250Xi, Thermo Scientific).

Electrochemical performance test

A 2032 button cell was packaged in a glove box full of Ar to study the Li storage properties of MnO_2 and MnO_2 -Au. Firstly, a certain amount of carboxymethyl cellulose (CMC), conductive carbon black (super P), and active material was mixed to form a slurry, which was evenly spread on the copper foil. The commercial lithium salt (LiPF_6) (0.1 M) in the mixed solvent of ethylene carbonate (EC) and diethyl carbonate (DEC) served as the electrolyte. The pure Li Foil and Celgard-2400 were the cathode and the separator, respectively. The rate performance, long cycle performance, galvanostatic charge/discharge (GCD), and galvanostatic intermittent titration technique (GITT) tests were conducted on the battery test system (LAND-CT2001A). The cyclic voltammetry curve (CV) of the battery was collected by the CHI760E electrochemical workstation. The AC impedance testing (EIS) was conducted at the Electrical workstation (Princeton ParSTAT MC) with an amplitude of 5 mV.

Ultrasonic detection

The nonlinear ultrasonic testing system used is RAM-5000 SNAP (RITEC Inc., Warwick, RI), which reflects material seat damage by studying the nonlinear effects of waves. It has the function of measuring ultrasonic attenuation and wave velocity. Compared with traditional linear ultrasonic testing methods, RAM-5000 has higher sensitivity. The center frequency of the transducer is 250 kHz, and the incident angle of the wave is adjusted to ensure that the incident wave is a Lamb wave. Lamb waves can detect small defects, cracks, or other damages in structures and have unique advantages in structural health monitoring and non-destructive testing. Therefore, these waves are used for ultrasonic testing here. Glycerin is used as the ultrasonic coupling agent, and the piezoelectric ceramic plate receives the Lamb wave signal. Five representative batteries were measured, namely, the newly installed battery with a short circuit, the battery with a short circuit after a long cycle, the initial state of a normal battery, the fully charged state of a normal battery, and the fully discharged state of a normal battery named as Sample 1, Sample 2, Sample 3, Sample 4, and Sample 5, respectively. The ultrasonic coefficient can be obtained from the time domain signals of different primary frequencies.

RESULTS AND DISCUSSION

The crystal phase and composition of the MnO₂-Au were determined by XRD. The XRD pattern is composed of the diffraction peaks of tetragonal MnO₂ (JCPDF No.24-0735) and the cubic Au (JCPDF No.040784) [Figure 1A]. It can be seen that the diffraction peaks of MnO₂-Au and the standard diffraction peaks can be well matched, indicating that the two materials are formed by self-assembly. There are no other miscellaneous peaks in the spectrogram, indicating that the product MnO₂ has a high purity. In addition, the sharp peaks suggest the crystallinity of the MnO₂-Au is very good. The XRD patterns of MnO₂-Au synthesized in water solutions with various concentration ratios of NaBH₄ and HAuCl₄ have been displayed in Figure 1B. The diffraction peak of Au is gradually enhanced with the increased HAuCl₄ content. As depicted in low-magnification and high-magnification SEM images [Figure 1C and D], the synthesized MnO₂ has a rod-like structure and presents a porous network distribution. Each nanorod has a length of 1-2 μm and a diameter of 50 to 100 nm. The Au nanoparticles are stuck on the surface of the rod-shaped MnO₂ [Figure 1D]. The XPS spectra of MnO₂-Au are displayed in Figure 2. The peaks of Au 4f_{5/2} and Au 4f_{7/2} in MnO₂-Au samples are 87.35 and 83.89 eV, respectively, demonstrating that Au presents in the form of metal^[27,28]. The distance between the Au 4f_{7/2} peak and the Au standard binding energy is 0.11 eV, which is because of the interaction between MnO₂ nanorods and Au nanoparticles. The XPS spectra for O 1s and Mn 2p of MnO₂ in the prepared sample are exhibited in Figure 2B and C. The binding energy difference between the two valence peaks of Mn 2p_{3/2} and Mn 2p_{1/2} is 11.8 eV, which represents the unique spin separation energy in MnO₂^[29]. The XPS spectrum for O 1s is divided into three parts, representing the Mn-O-H bond, Mn-O bond, and H-O-H bond, respectively. The interior of the sample is rich in oxygen vacancies, which can increase the conductivity of the material^[30,31].

CV curves of MnO₂-Au samples were acquired at 0.1 mV s⁻¹ [Figure 3A]. Two obvious redox peaks are located at 0.35 and 1.3 V, respectively. It can be clearly observed that after the first cycle, there is a significant decrease in reversible capacity. This is due to irreversible reactions occurring on the surface of the material, forming a solid electrolyte interface and reducing the reversible capacity of MnO₂-Au. So, during the third week of the cycle, there was severe capacity degradation^[4,32]. Except for the first cycle, the CV curves are overlapped, suggesting that the MnO₂-Au sample has good reversibility and stability^[33]. To study the influence of self-assembled MnO₂-Au on the performances of Li-ion batteries, the electrochemical performances of MnO₂ and MnO₂-Au anode have been characterized. As shown in Figure 3B, MnO₂-Au exhibits ultra-high specific capacity at different charge-discharge rates, especially at high rates. Additionally, when the rate is restored to 0.03 C, the capacity of the MnO₂-Au anode can be almost completely recovered. MnO₂-Au also plays a prominent role in the long-term cycle performance of Li-ion batteries. After 500 cycles, the specific capacity of MnO₂-Au is 428.3 mAh/g, while the specific capacity of MnO₂ is only 393.6 mAh/g. The battery still maintains a very high-capacity retention rate [Figure 3C]. Nyquist plots of the two electrode materials are exhibited in Figure 3D. Compared to MnO₂, MnO₂-Au has a lower charge transfer resistance, indicating that the MnO₂-Au heterojunction facilitates the diffusion of Li⁺ and electrons at the electrolyte/electrode interface^[34,35]. The causes of the accelerated transportation kinetics of the MnO₂-Au anode had been further inquired by GITT [Figure 4].

Through testing these five different types of batteries, it was found that the newly installed short-circuit battery had the highest normalized ultrasonic nonlinear coefficient. The nonlinear coefficient of the short-circuit battery after a long cycle decreased to a certain extent, and the nonlinear coefficient of the initial state battery further decreased. During the charging/discharging process, the nonlinear coefficient in the fully charged state had a certain degree of improvement compared to the initial state. Moreover, the normalized

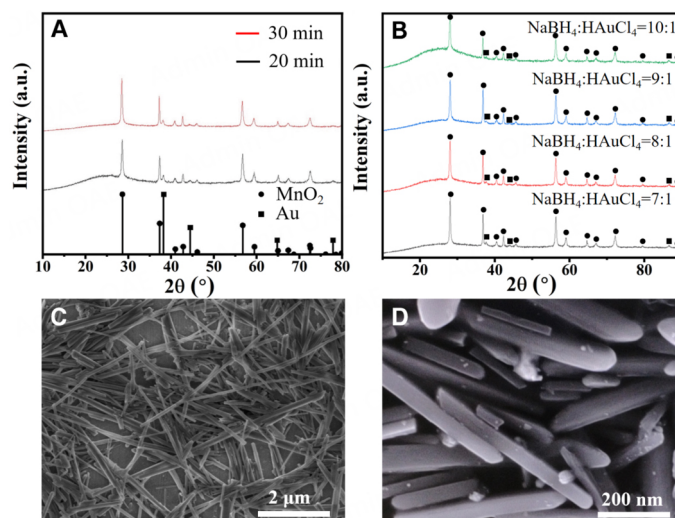


Figure 1. (A) XRD patterns of MnO₂-Au under ultrasound for 30 min (red line) and ultrasound for 20 min (black line). (B) XRD patterns of MnO₂-Au under different concentration ratios of NaBH₄ and HAuCl₄. SEM images of MnO₂-Au (C and D).

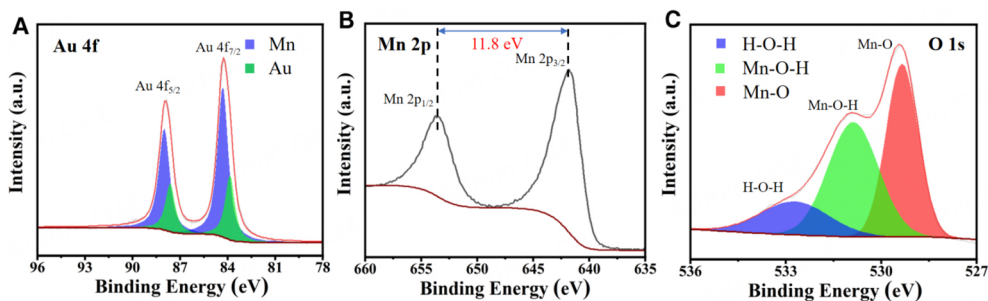


Figure 2. XPS spectra for Au 4f (A), Mn 2p (B), and O 1s (C) in MnO₂-Au materials.

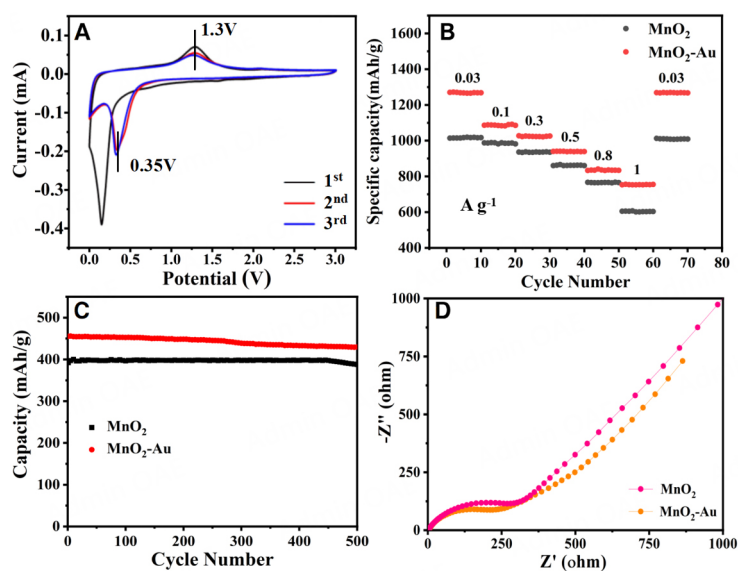


Figure 3. (A) CV curves of MnO₂-Au sample at 0.1 mV s⁻¹. Rate performances (B), long cycle performances (C), and Nyquist plots (D) of MnO₂ and MnO₂-Au anodes.

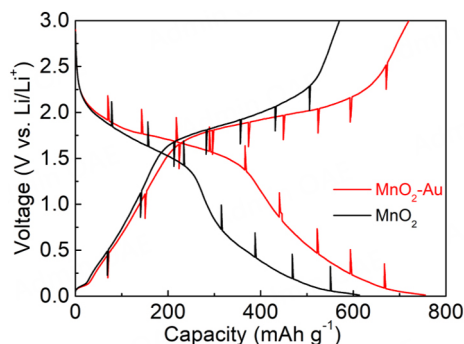


Figure 4. GITT plots of MnO_2 and MnO_2 -Au anodes.

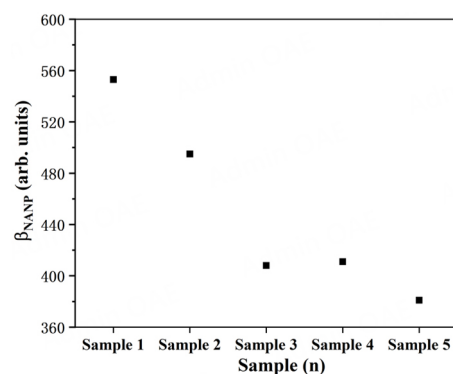


Figure 5. Normalized ultrasonic nonlinear coefficient of batteries in different states.

ultrasonic nonlinear coefficient in the fully discharged state further decreased to 381 [Figure 5]. The above phenomenon may be caused by the following reasons: during the charging/discharging process, the lithiation and delithiation of the active materials are completed through the following methods, including intercalation, deintercalation, and phase transition^[36,37]. The lithiation and delithiation of the active materials are non-equilibrium processes, which can lead to the generation of Li-ion concentration gradients in the active material. The Li-ion concentration gradients can cause tensile or compressive stress inside the active material^[38]. Taking spherical particles of the active materials as an example, when Li ions enter the outer surface of the particles, the concentration of these ions near the particle surface is much higher than that of near the center, resulting in an obvious difference in Li-ion concentration between the outer surface and the center particles^[39]. When the Li-ion content near the surface increases, the material will expand. However, the delithiated material near the center will suppress this expansion, causing the surface material to withstand compressive stress while the center material begins to withstand tensile stress^[40]. On the contrary, when lithiated particles are delithiated, the particle surface undergoes tensile stress (relative to the particle center of mass), which may lead to cracks on the surface, resulting in the changes in the normalized ultrasonic nonlinear coefficient^[41,42].

CONCLUSIONS

In summary, the hetero-structured MnO_2 -Au Li-ion battery anode has been constructed with high capacities and superior rate performances. The Au nanoparticles are attached to the MnO_2 nanorods by epitaxial growth so that they have excellent electrochemical properties. This is attributed to the fact that this heterostructure can induce the aggregation of charges, enhance the mobility of electrons and ions, and, thus, achieve higher rate performance. Finally, the ultrasonic testing to determine the battery in different states

has been conducted. The different ultrasonic nonlinear coefficients of the five different states of batteries have been obtained. Short-circuited batteries have the highest nonlinear coefficient, while after long cycles, they have the lowest nonlinear coefficient. The nonlinear coefficient of batteries in different charging and discharging states is in the middle. Ultrasonic testing of Li batteries has advantages such as non-invasive and high detection accuracy, which can safely and accurately evaluate the internal structure and condition of the battery, providing important support for early detection of problems and prediction of lifespan.

DECLARATIONS

Authors' contributions

Made substantial contributions to the conception and design of the study and performed data analysis and interpretation: An C, Wang S, Lin L, Ding X

Conducted data acquisition and provided administrative, technical, and material support: An C, Wang S, Deng Q, Hu N

Availability of data and materials

The data and materials can be obtained by requested.

Financial support and sponsorship

This work was supported by the Research Program of Local Science and Technology Development under the Guidance of Central (216Z4402G), the National Natural Science Fund of China (Grant No. 12172118 and No. 12172205), and the Science Research Project of Hebei Education Department (BJK2022015). We also acknowledge support from the “Yuanguang” Scholar Program of Hebei University of Technology.

Conflicts of interest

All authors declared that there are no conflicts of interest.

Ethical approval and consent to participate

Not applicable.

Consent for publication

Not applicable.

Copyright

© The Author(s) 2024.

REFERENCES

1. Ming J, Li M, Kumar P, Li LJ. Multilayer approach for advanced hybrid lithium battery. *ACS Nano* 2016;10:6037-44. [DOI](#) [PubMed](#)
2. Ma Y, Ma J, Cui G. Small things make big deal: Powerful binders of lithium batteries and post-lithium batteries. *Energy Stor Mater* 2019;20:146-75. [DOI](#)
3. Zhou D, Zheng W, Chen S, et al. Research on state of health prediction model for lithium batteries based on actual diverse data. *Energy* 2021;230:120851. [DOI](#)
4. An C, Li Y, Wu S, et al. Matched MnO@C anode and porous carbon cathode for Li-ion hybrid supercapacitors. *Rare Met* 2023;42:1959-68. [DOI](#)
5. Chen Z, Li S, Cai X, Zhou N, Cui J. Online state of health monitoring of lithium-ion battery based on model error spectrum for electric vehicle applications. *J Energy Stor* 2022;45:103507. [DOI](#)
6. Li Q, Liu Y, Zhang Z, et al. Construction of dynamic alloy interfaces for uniform Li deposition in Li-metal batteries. *Energy Environ Mater* 2023:e12618. [DOI](#)
7. Pradhan SK, Chakraborty B. Battery management strategies: an essential review for battery state of health monitoring techniques. *J Energy Stor* 2022;51:104427. [DOI](#)
8. Wang S, Takyi-aninakwa P, Jin S, Yu C, Fernandez C, Stroe D. An improved feedforward-long short-term memory modeling method for the whole-life-cycle state of charge prediction of lithium-ion batteries considering current-voltage-temperature variation. *Energy*

- 2022;254:124224. DOI
9. Wang S, Wu F, Takyi-aninakwa P, Fernandez C, Stroe D, Huang Q. Improved singular filtering-Gaussian process regression-long short-term memory model for whole-life-cycle remaining capacity estimation of lithium-ion batteries adaptive to fast aging and multi-current variations. *Energy* 2023;284:128677. DOI
 10. Nie Y, Wang Y, Li L, Liao H. Literature review on power battery echelon reuse and recycling from a circular economy perspective. *Int J Environ Res Public Health* 2023;20:4346. DOI PubMed PMC
 11. Wang M, Liu K, Dutta S, et al. Recycling of lithium iron phosphate batteries: status, technologies, challenges, and prospects. *Renew Sustain Energy Rev* 2022;163:112515. DOI
 12. Lelie M, Braun T, Knips M, et al. Battery management system hardware concepts: an overview. *Appl Sci* 2018;8:534. DOI
 13. Wang Y, Tian J, Sun Z, et al. A comprehensive review of battery modeling and state estimation approaches for advanced battery management systems. *Renew Sustain Energy Rev* 2020;131:110015. DOI
 14. Wu Y, Wang Y, Yung WKC, Pecht M. Ultrasonic health monitoring of lithium-ion batteries. *Electronics* 2019;8:751. DOI
 15. Robinson JB, Maier M, Alster G, Compton T, Brett DJL, Shearing PR. Spatially resolved ultrasound diagnostics of Li-ion battery electrodes. *Phys Chem Chem Phys* 2019;21:6354-61. DOI PubMed
 16. Bieker G, Winter M, Bieker P. Electrochemical in situ investigations of SEI and dendrite formation on the lithium metal anode. *Phys Chem Chem Phys* 2015;17:8670-9. DOI PubMed
 17. Jayasubramanian S, Lee HW. Directing battery chemistry using side-view operando optical microscopy. *Korean J Chem Eng* 2023;40:488-96. DOI
 18. Steiger J, Richter G, Wenk M, Kramer D, Mönig R. Comparison of the growth of lithium filaments and dendrites under different conditions. *Electrochem Commun* 2015;50:11-4. DOI
 19. Yin T, Jia L, Li X, Zheng L, Dai Z. Effect of high-rate cycle aging and over-discharge on NCM811 (LiNi_{0.8}Co_{0.1}Mn_{0.1}O₂) batteries. *Energies* 2022;15:2862. DOI
 20. Cai Z, Pan T, Jiang H, Li Z, Wang Y. State-of-charge estimation of lithium-ion batteries based on ultrasonic detection. *J Energy Stor* 2023;65:107264. DOI
 21. Chandrashekar S, Trease NM, Chang HJ, Du LS, Grey CP, Jerschow A. ⁷Li MRI of Li batteries reveals location of microstructural lithium. *Nat Mater* 2012;11:311-5. DOI PubMed
 22. Louli AJ, Eldesoky A, Weber R, et al. Diagnosing and correcting anode-free cell failure via electrolyte and morphological analysis. *Nat Energy* 2020;5:693-702. DOI
 23. Wu H, Zhuo D, Kong D, Cui Y. Improving battery safety by early detection of internal shorting with a bifunctional separator. *Nat Commun* 2014;5:5193. DOI PubMed
 24. Deng Z, Huang Z, Shen Y, et al. Ultrasonic scanning to observe wetting and “unwetting” in Li-ion pouch cells. *Joule* 2020;4:2017-29. DOI
 25. Davies G, Knehr KW, Van Tassell B, et al. State of charge and state of health estimation using electrochemical acoustic time of flight analysis. *J Electrochem Soc* 2017;164:A2746. DOI
 26. Zhang K, Yin J, He Y. Acoustic emission detection and analysis method for health status of lithium ion batteries. *Sensors* 2021;21:712. DOI PubMed PMC
 27. Guan DH, Wang XX, Li F, et al. All-solid-state photo-assisted Li-CO₂ battery working at an ultra-wide operation temperature. *ACS Nano* 2022;16:12364-76. DOI
 28. Wang B, Yue Y, Pang X, et al. Nature of HCl oxidation Au anomalies and activation of non-carbon-material-supported Au catalyst. *J Catal* 2021;404:198-203. DOI
 29. Wu Y, Xu Z, Ren R, et al. Flexible ammonium-ion pouch cells based on a tunneled manganese dioxide cathode. *ACS Appl Mater Interfaces* 2023;15:12434-42. DOI
 30. Chen B, Miao H, Hu R, et al. Efficiently optimizing the oxygen catalytic properties of the birnessite type manganese dioxide for zinc-air batteries. *J Alloys Compd* 2021;852:157012. DOI
 31. Ni Z, Liang X, Zhao L, Zhao H, Ge B, Li W. Tin doping manganese dioxide cathode materials with the improved stability for aqueous zinc-ion batteries. *Mater Chem Phys* 2022;287:126238. DOI
 32. Zhang X, Li S, Wang S, Du S, Wen Z, Sun J. Amorphization improving the initial capacity decay of MnO₂ anode material for LIBs. *Chem Phys Lett* 2022;786:139200. DOI
 33. Hu S, Liu X, Wang C, Camargo PHC, Wang J. Tuning thermal catalytic enhancement in doped MnO₂-Au nano-heterojunctions. *ACS Appl Mater Interfaces* 2019;11:17444-51. DOI
 34. He T, Feng J, Ru J, Feng Y, Lian R, Yang J. Constructing heterointerface of metal atomic layer and amorphous anode material for high-capacity and fast lithium storage. *ACS Nano* 2019;13:830-8. DOI PubMed
 35. Qiao H, Liu H, Huang Z, et al. Black phosphorus nanosheets modified with Au nanoparticles as high conductivity and high activity electrocatalyst for oxygen evolution reaction. *Adv Energy Mater* 2020;10:2002424. DOI
 36. Gupta D, Koenig GM. Analysis of chemical and electrochemical lithiation/delithiation of a lithium-ion cathode material. *J Electrochem Soc* 2020;167:020537. DOI
 37. Lu Y, Li J, Zhao Y, Zhu X. Lithium clustering during the lithiation/delithiation process in LiFePO₄ Olivine-structured materials. *ACS Omega* 2019;4:20612-7. DOI PubMed PMC
 38. Liu P, Sridhar N, Zhang Y. Lithiation-induced tensile stress and surface cracking in silicon thin film anode for rechargeable lithium

- battery. *J Appl Phys* 2012;112:093507. [DOI](#)
39. Galluzzo MD, Loo WS, Schaible E, Zhu C, Balsara NP. Dynamic structure and phase behavior of a block copolymer electrolyte under dc polarization. *ACS Appl Mater Interfaces* 2020;12:57421-30. [DOI](#) [PubMed](#)
 40. Zhang P, Wang Q, Qiu W, Feng L. Diffusion and induced stress tuning mechanisms: analytical modeling of species transport in silicon-graphene layered composite electrodes for lithium batteries. *J Electrochem Soc* 2023;170:050508. [DOI](#)
 41. Basu S, Koratkar N, Shi Y. Structural transformation and embrittlement during lithiation and delithiation cycles in an amorphous silicon electrode. *Acta Mater* 2019;175:11-20. [DOI](#)
 42. Larsson C, Larsson F, Xu J, Runesson K, Asp LE. Effects of lithium insertion induced swelling of a structural battery negative electrode. *Compos Sci Technol* 2023;244:110299. [DOI](#)